Pergamon

Computers Math. Applic. Vol. 36, No. 7, pp. 69–78, 1998

Printed in Great Britain
0898-1221/98 $19.00 + 0.00

PII: S0898-1221(98)00173-4

Numerical Solutions of Differential Equations for Renal Concentrating Mechanism in Inner Medullary Vasa Recta Models

I. H. MOON AND R. P. TEWARSON*
Institute of Mathematical Modeling
Department of Applied Mathematics and Statistics
State University of New York
Stony Brook, N.Y. 11794-3600, U.S.A.

(Received February 1998; accepted March 1998)

Abstract—Two vasa recta models of the renal concentrating mechanism are presented. It is shown that by considering the effects of ascending vasa recta permeabilities, interstitial resistance, lateral small scale histotopography, and standard deviations in permeability values, these models lead to significant improvements in collecting duct urea and salt concentration ratios. © 1998 Elsevier Science Ltd. All rights reserved.

Keywords—Differential equations, Numerical methods, Kidney models.

1. INTRODUCTION

The composition of body fluids of mammals is maintained within very narrow limits. One of the primary organs for this purpose is the kidney.

A lengthwise cross-section of the kidney reveals two distinct regions: the *cortex* and the *medulla* (see Figures 1 and 2). The *medulla* is further subdivided into the *outer* and *inner parts*; and it contains the loops of Henle (which turn at different levels) and the collecting ducts. The renal corpuscles, and the proximal and the distal tubules reside in the *cortex*. Blood enters the kidney and is filtered at the renal corpuscle. The resulting ultrafiltrate then flows successively through the proximal tubule (which winds around the renal corpuscle), Henle's loop (the descending (DHL) and ascending (AHL) parts are joined by a hairpin turn), the distal tubule (which winds around in the cortex and makes contact with the *Juxta-glomerular apparatus* related to the renal corpuscle), and the Collecting Duct (CD) which is connected to the *renal pelvis*. The ultrafiltrate then enters the *ureter*, empties into the *bladder*, and finally exits the body through the *urethra* as *urine*. The final urine may be either more or less concentrated than plasma or other body fluids. Until the ultrafiltrate reaches the renal pelvis, the tubules (proximal tubule, Henle's loop, distal tubule, and collecting duct) may selectively exchange solutes and water through the tubule walls with the surrounding interstitium. Blood also flows down into the medulla and then back to the cortex through the *vasa recta* (DVR and AVR). This retrieves the water and solutes absorbed from the tubules. This selective reabsorption and secretion adjusts the composition

*Research supported by NIH Grant DK17593.
The authors wish to thank M. Marcano for his helpful suggestions.

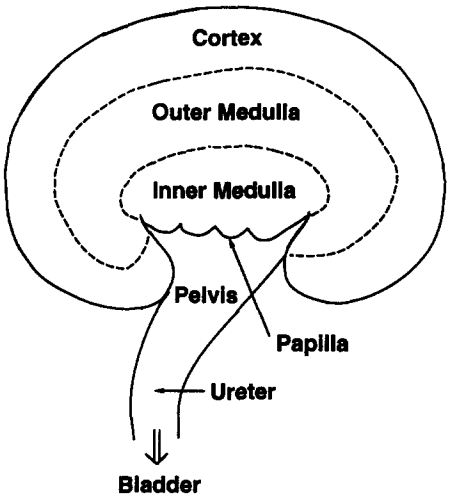

Figure 1. Kidney cross section.

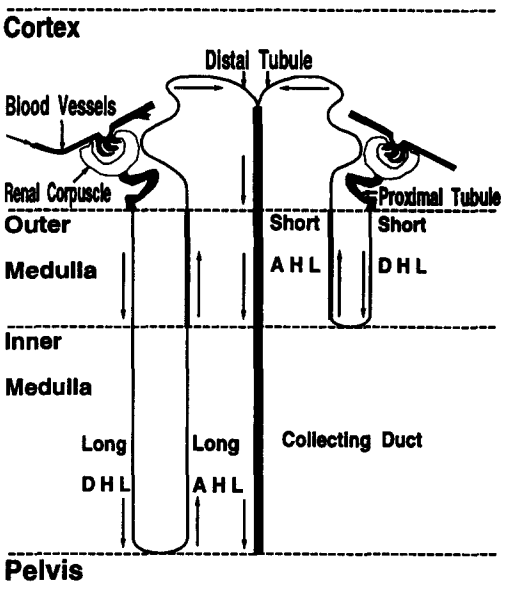

Figure 2. Schematic of nephrons and collecting duct.

of the interstitial fluid bathing the cells of the body. This fluid is maintained within the strict tolerances necessary for life. See [1–7] for more details and an extensive list of references.

Mathematical models are necessary in the testing many of the basic ideas leading to our understanding of renal concentrating mechanism [8–14]. Computer models that use experimentally available parameters have generated concentration gradients in the outer medulla but not in the inner medulla. How the inner medulla concentrates urine is still one of the major unsolved problems in renal physiology.

In this paper, we describe two models M1 (Figure 3) and M2 (Figure 4). M1 results by incorporating, in our seven tube vasa recta model [14] (called M0 in the present paper), more realistic and comprehensive direct interactions between each of the tubes (DHL, AHL, and CD) and the vasa recta (AVR's). M2 is a result of allowing, in M1, preferential interaction between each of the tubes (DHL, AHL, and CD) and the vasa recta (DVR). The role of interstitium and permeability ramps is also investigated. In our previous paper [14], we showed that, if suitable modifications are made to a few carefully selected subset of the parameters, then the vasa recta models lead to the same osmolality and concentration ratios as our central core models [11,12,15]. In the present paper, we show that by choosing the permeabilities within the ranges of experimentally known results and realistic input values, all models (M0, M1, and M2) yield concentration ratios for the CD that are closer to the experimental values than the values obtained

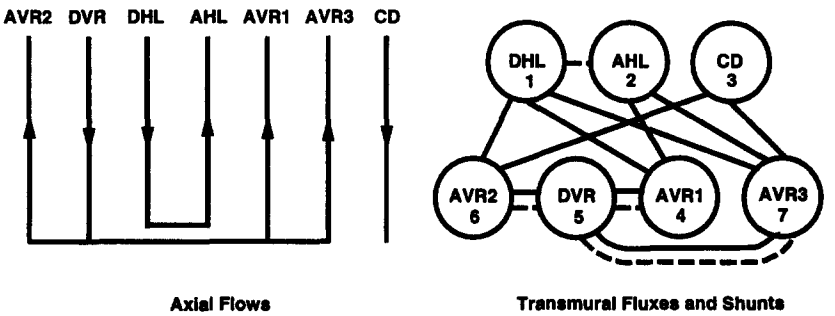

Figure 3. Seven tuber model (M1).

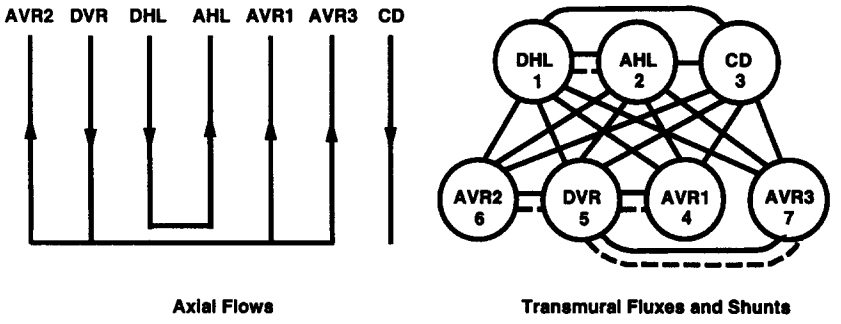

Figure 4. Seven tube model with preferential interaction (M2).

from past models. The salt and urea concentrations of the output from CD are well within the ranges of values given in [16].

2. SEVEN TUBE MODEL (M1)

In most of the current models, the primary reason for having DHL, AHL, and CD interact transmurally with only AVR's is due to the relatively large permeabilities of AVR's. In view of the available pictures of the cross sections of the inner medulla (for example see [5, p. 540, Figure 1d]), it seems reasonable to consider the relative proximity of other tubes. Therefore, adding more transmural fluxes to our earlier model M0 (see [14, Figure 3]), we get model M1, shown in Figure 3. In this model, DHL now interacts, not only, with AVR1 and AVR3, but also, with AVR2. New transmural interactions between CD and AVR2 have also been included.

Let $i = 1, 2, 3, 4, 5, 6$, and 7 denote, respectively, DHL, AHL, CD, AVR1, DVR, AVR2, and AVR3, and x be the distance measured from the top ($x = 0$) to the bottom ($x = 1$) of the inner medulla. The variables are: $F_{iv}(x)$ = axial volume flows, $C_{ik}(x)$ = solute concentrations, where $k = s$ (salt), u (urea). The entering flows and concentrations $F_{iv}(0)$, $C_{ik}(0)$, $i = 1, 3, 5$, $k = s, u$ are given. At $x = 1$, DHL (Tube 1) makes a hairpin turn to become AHL (Tube 2) and, therefore, $F_{2v}(1) = -F_{1v}(1)$ and $C_{2k}(1) = C_{1k}(1)$. Also, at $x = 1$, DVR (Tube 5) makes a hairpin turn to become AVR1 (Tube 4), AVR2 (Tube 6), and AVR3 (Tube 7), and, therefore, $C_{4k}(1) = C_{5k}(1) = C_{6k}(1) = C_{7k}(1)$, $F_{4v}(1) = -\gamma_4 F_{5v}(1)$, $F_{7v}(1) = -\gamma_7 F_{5v}(1)$, and $F_{6v}(1) = -(1 - \gamma_4 - \gamma_7)F_{5v}(1)$, where γ_4 and γ_7 are, respectively, the fractions of DVR volume flow going to AVR1 and AVR3.

The differential equations are [14]

$$\frac{dF_{iv}}{dx} + J_{iv}(x) = 0, \tag{1}$$

$$\frac{d(F_{iv}C_{ik})}{dx} + J_{ik}(x) = 0, \tag{2}$$

$$\frac{dF_{ik}}{dx} + J_{ik}(x) = 0, \tag{3}$$

where $J_{iv}(x)$ and $J_{ik}(x)$ are, respectively, transmural volume and solute fluxes. $J_{iv}(x)$ and $J_{ik}(x)$ are functions of only $C_{ik}(x)$, $i = 1, 2, 3, 5$, and $C_{av,k}(x)$, $av = 4, 6, 7$. We have

$$J_{iv}(x) = h_{iv}(x) \sum_k RT[C_{av,k}(x) - C_{ik}(x)]\sigma_{ik}(x), \qquad k = s, u, \tag{4}$$

$$J_{ik}(x) = J_{iv}(x)[1 - \sigma_{ik}(x)]\frac{C_{ik}(x) + C_{av,k}(x)}{2} + h_{ik}(x)[C_{ik}(x) - C_{av,k}(x)], \quad k = s, u, \tag{5}$$

where σ_{ik} is the Staverman reflection coefficient of the wall of the i^{th} tube for the k^{th} solute, h_{ik} is its passive permeability for the k^{th} solute, h_{iv} is its hydraulic permeability coefficient, R is the gas constant, and T is the absolute temperature.

Mass balance requires that

$$\sum_{i=1}^{7} J_{iv}(x) = 0, \qquad \sum_{i=1}^{7} J_{ik}(x) = 0. \tag{6}$$

If we set $h = 1/n$, $x_j = (j-1)h$, where $j = 1, \ldots, n+1$; $F_{ivj} = F_{iv}(x_j), F_{ikj} = F_{ik}(x_j)$, and $C_{ikj} = C_{ik}(x_j)$, then, as shown in [17], integrating (1)–(3) and using the boundary conditions we get a system of nonlinear algebraic equations, which can be written as

$$f(y, z) = 0, \tag{7}$$

$$g(y, z) = 0, \tag{8}$$

where $y = (C_{ikj})$, $i = 1, 2, 3$, $k = s, u$; for $i = 1, 3$, $j = 2, \ldots, n+1$ and for $i = 2$, $j = n$, $n-1$, $\ldots, 1$; $z = (F_{5vj}, C_{ikj})$, $k = s, u$; for $i = 4, 6, 7$, $j = 1, \ldots, n$, and for $i = 5$, $j = 2, \ldots, n+1$. Therefore, in equations (7) and (8), for this model, $f, y \in R^{6n}$ and $g, z \in R^{9n}$. The basic equations and variables are the ones associated with DVR, AVR1, AVR2, and AVR3.

As shown in [17] and [18], the nonbasic variables y are expressed as a functions of the basic variables z by solving the nonbasic equations $f(y(z), z) = 0$ for $y(z)$. This leads to an efficient algorithm for the basic equations $g(y(z), z) = 0$ for z.

3. SEVEN TUBE MODEL WITH PREFERENTIAL INTERACTION (M2)

By considering the total transmural connectivity between all tubes, we get the model shown in Figure 4. For this model, we let $y = (C_{ikj})$, $i = 1, 2, 3, 4, 5, 6, 7$, $k = s, u$; for $i = 1, 3, 5$, $j = 2, \ldots, n+1$, and for $i = 2, 4, 6, 7$, $j = n, n-1, \ldots, 1$; $z = (F_{5vj}, C_{ikj})$, $k = s, u$; for $i = 2, 4, 6, 7$, $j = 1, \ldots, n$, and for $i = 1, 3, 5$, $j = 2, \ldots, n+1$. Therefore, in equations (7) and (8), nonbasic equations and variables $f, y \in R^{14n}$ and basic equations and variables $g, z \in R^{15n}$.

Using the picture of the cross section of the inner medulla [5], we define a *distance function* A_{pij}, between the p^{th} and i^{th} tubes at the j^{th} level, to calculate the transmural fluxes. The rationale for doing this is given in [5].

> "The importance of axial and lateral compartmentalization of the medulla in general for the process urine concentration seems indisputable, ... Our fundamental assumption is that patterns of solute and water exchange among tubules and vessels in the IM are determined not only by specific membrane permeabilities and concentration differences but also by the small scale histotopography of the region. As a result of their locations either distant from one another or on opposite sides of interposed structures, the likelihood of significant solute or water exchange between some tubules and vessels is decreased (that is, they are separated from each other). Since the AVR are net reabsorbers of water—having significant exchange not just with DVR (in classical countercurrent exchange), but also with CD and possibly DHL—their interposition between other structures could influence water and (indirectly) solute exchanges."

The formulas for the distance functions for DHL were derived as follows. Let A_{1i}, $i = 2, 3, 4, 5, 6, 7$, be the relative distances between DHL and the i^{th} tube (obviously, $i \neq 1$). From [4,19], the number of loops (in CD and vasa recta) has to be equal to the value of distance function for DHL (AHL, CD, and vasa recta) at each level j, let

$$\sum_{i=2}^{7} A'_{1ij} = nlp_j, \tag{9}$$

$$T_1 = \sum_{i=2}^{7} A_{1i}^{-1}, \qquad A'_{1ij} = A_{1i}^{-1} nlp_j \alpha, \tag{10}$$

where α is a proportionality constant, nlp_j is the number of loops at level j, and therefore, from (9) and (10),

$$A'_{1ij} = A_{1i}^{-1} nlp_j \frac{1}{T_1}, \qquad i = 2,3,4,5,6,7. \tag{11}$$

Now, we derive formulas for AHL. Let A_{2i}, $i = 1,3,4,5,6,7$, be the relative distances between AHL and other tubes i. Let

$$\sum_{i=3}^{7} A'_{2ij} = nlp_j - A'_{21j}, \qquad A'_{21j} = A'_{12j}, \tag{12}$$

$$T_2 = \sum_{i=3}^{7} A_{2i}^{-1}, \qquad A'_{2ij} = A_{2i}^{-1} nlp_j \delta, \tag{13}$$

where δ is a proportionality constant and A'_{2ij} is the value of distance function at each level for AHL. From (12) and (13),

$$\sum_{i=3}^{7} A_{2i}^{-1} nlp_j \delta = nlp_j - A'_{21j}, \tag{14}$$

$$nlp_j \delta = \left[nlp_j - A'_{21j} \right] \frac{1}{T_2}. \tag{15}$$

Therefore,

$$A'_{2ij} = A_{2i}^{-1} \left[nlp_j - A'_{21j} \right] \frac{1}{T_2}, \qquad i = 3,4,5,6,7. \tag{16}$$

Next, we derive formulas for CD. Let A_{3i}, $i = 1,2,4,5,6,7$, be the relative distances between CD and other tubes i. Let

$$\sum_{i=4}^{7} A'_{3ij} = ncd_j - A'_{31j} - A'_{32j}, \qquad A'_{31j} = A'_{13j}, \qquad A'_{32j} = A'_{23j}, \tag{17}$$

$$T_3 = \sum_{i=4}^{7} A_{3i}^{-1}, \qquad A'_{3ij} = A_{3i}^{-1} ncd_j \gamma, \tag{18}$$

where γ is a proportionality constant, ncd_j is the number of CD's at level j, and A'_{3ij} is the value of distance function at each level for CD. From (17) and (18),

$$\sum_{i=4}^{7} A_{3i}^{-1} ncd_j \gamma = ncd_j - A'_{31j} - A'_{32j}, \tag{19}$$

$$ncd_j \gamma = \left[ncd_j - A'_{31j} - A'_{32j} \right] \frac{1}{T_3}. \tag{20}$$

Therefore,

$$A'_{3ij} = A_{3i}^{-1} \left[ncd_j - A'_{31j} - A'_{32j} \right] \frac{1}{T_3}, \qquad i = 4,5,6,7. \tag{21}$$

Formulas for DVR can be derived in a similar manner. A'_{5ij}, values of distance function at each level for DVR, are

$$A'_{5ij} = A_{5i}^{-1} \left[nvr_j - A'_{51j} - A'_{52j} - A'_{53j} \right] \frac{1}{T_5}, \qquad i = 4,6,7, \tag{22}$$

where nvr_j is the number of vasa recta at level j, and

$$T_5 = A_{54}^{-1} + A_{56}^{-1} + A_{57}^{-1}, \tag{23}$$

$$A'_{51j} = A'_{15j}, \qquad A'_{52j} = A'_{25j}, \qquad A'_{53j} = A'_{35j}, \tag{24}$$

Table 1. Relative distances A_{pi} for M2.

	DHL (1)	AHL (2)	CD (3)	DVR (5)	AVR1 (4)	AVR2 (6)	AVR3 (7)
DHL (1)	–	1.5	2.5	1.5	1.0	2.5	2.0
AHL (2)	–	–	1.5	3.0	1.0	1.5	3.0
CD (3)	–	–	–	4.0	2.0	1.0	4.0
DVR (5)	–	–	–	–	2.0	4.5	1.0
AVR1 (4)	–	–	–	–	–	2.0	2.0
AVR2 (6)	–	–	–	–	–	–	4.0

Table 2. Parameter values with standard deviations.

	Unnormalized Values				
	$h_w \times 10^{-5}$	$h_s \times 10^{-5}$	$h_u \times 10^{-5}$	σ_s	σ_u
DHL - Upper	25.08 ± 6.47	3.50 ± 1.2	13.50 ± 6.5	0.99 ± 0.04	0.97 ± 0.04
- Lower	25.08 ± 6.47	3.50 ± 1.2	13.50 ± 6.5	0.99 ± 0.04	0.97 ± 0.04
AHL - Upper	0.18 ± 0.144	79.60 ± 3.6	22.80 ± 4.5	1	1
- Lower	0.18 ± 0.144	79.60 ± 3.6	22.80 ± 4.5	1	1
CD - Upper	1.095 ± 0.37	0.00	4.10 ± 0.7	1.00 ± 0.05	1
- Lower	1.535 ± 0.24	1.18 ± 0.24	69.20 ± 15.2	1.00 ± 0.05	1
DVR - Upper	106.40	75.00 ± 10.00	76.00 ± 11.00	0.017	0.07
- Lower	106.40	75.00 ± 10.00	76.00 ± 11.00	0.017	0.07

Table 3. Unnormalized and normalized parameter values.

	Unnormalized Values			Normalized Values				
	$h_w \times 10^{-5}$	$h_s \times 10^{-5}$	$h_u \times 10^{-5}$	h_w	h_s	h_u	σ_s	σ_u
DHL - Upper	25.2508	3.50	13.635	0.0049119	0.5174388	2.0157937	0.99	0.97
- Lower	25.08	3.50	13.50	0.0048787	0.5174388	1.9958353	0.99	0.97
AHL - Upper	0.18	79.60	22.572	0.0000350	11.768037	3.3370367	1.00	1.00
- Lower	0.18	79.60	22.80	0.0000350	11.768037	3.3370367	1.00	1.00
CD - Upper	1.095	0.00	4.10	0.0003195	0.0	0.9092139	1.00	1.00
- Lower	1.535	1.18	69.20	0.0004479	0.2616762	15.345756	1.00	1.00
DVR - Upper	91.0313	75.75	74.25	0.0159372	10.078968	9.8793849	0.017	0.07
- Lower	90.13	75.00	75.00	0.0157794	9.9791767	9.9791767	0.017	0.07

where A_{5i}, $i = 4, 6, 7$, are the relative distances between DVR and i. The values for the relative distances between all tubes are shown in Table 1.

4. COMPUTATIONAL RESULTS

In Table 2, we have shown permeabilities and reflection coefficients. These values are readily available [20–27].

In Table 3, we show the unnormalized permeabilities (selected within the ranges of values in Table 2) and the corresponding normalized values. The normalization was done as follows. Let

$$N_i = \frac{2\pi l_i r_i}{F_{1v1}}, \qquad i = 1, \ldots, 5, \tag{25}$$

where l_i and r_i denote, respectively, the length and radius of the i^{th} tube, $i = 1, \ldots, 5$, and F_{1v1} is the amount of volume flow at the top ($x = 1$) of DHL. The normalized permeabilities are given by

$$h_{i,v,j}^{\text{norm}} = \frac{N_i h_{i,v,j}}{760}, \tag{26}$$

$$h_{i,k,j}^{\text{norm}} = N_i h_{i,k,j}, \qquad k = \text{salt, urea}. \tag{27}$$

Let h_{avw}, h_{avs}, and h_{avu} be AVR hydraulic, salt and urea permeabilities [1–5,22–25]. We used harmonic means [28], for calculating the composite permeabilities to account for the effect of AVR and interstitial permeabilities

$$h_{ip} = \frac{h_i h_p}{h_i + h_p}. \tag{28}$$

The composite reflection coefficients between two membranes were calculated by [29]

$$\sigma = \frac{\sigma_i h_p + \sigma_p h_i}{h_i + h_p}, \tag{29}$$

where σ_i and σ_p are the reflection coefficients, and h_i and h_p are permeabilities of the i^{th} and p^{th} membranes, respectively.

Let h_{Iw}, h_{Is}, and h_{Iu} be interstitial normalized hydraulic, salt and urea permeability functions. The rationale for using interstitial permeability functions is as follows. Interstitial spaces in the inner medulla are 15% by volume in rat, 20%–25% in rabbit at the top and 30% in rat, 40% in rabbit at the tip. Thus, there is approximately a two fold increase from the top of the inner medulla to its tip. It is pointed out in [4], that the interstitial cells are arranged like rungs of a ladder between parallel running tubules or vessels. In [2, Figure 12.8], light and electron micrographs of these lipid laden interstitial cells of the inner medulla are given. We posit that this inhibits, not only, axial diffusion in the interstitium, but also the transmural fluxes between tubules. The interstitial cells cover part of the tubule walls and it is also reasonable to assume that there is some resistance to lateral diffusion. Therefore, in order to approximate the effect of resistance to the lateral movement of water, salt and urea in the interstitium, we used the maximum permeabilities from all the tubes as approximations for the interstitial permeability functions.

Using the composite permeabilities (computed from Table 3), and the boundary values (estimated from [2,30]) shown in Table 4, we get the results in Table 5.

Table 4. Estimated boundary values from [2,30].

	DHL (1)	CD (3)	DVR (5)
Volume Flow, 10^{-7} ml/sec	1.76	0.12	2.16
NaCl Concentration, mmol/ml	0.212	0.117	0.053
Urea Concentration, mmol/ml	0.035	0.195	0.674

Table 5. Osmolality and conc. ratios using AVR permeabilities and interstitial permeability functions.

							DHL (Tube 1)			CD (Tube 3)		
	h_{avw}	h_{avs}	h_{avu}	h_{Iw}	h_{Is}	h_{Iu}	Osm.	Salt	Urea	Osm.	Salt	Urea
M1	∞	∞	∞	∞	∞	∞	1.873	1.231	9.946	1.928	2.199	1.633
	1185.0	125.0	131.0	∞	∞	∞	1.825	1.129	9.499	1.872	1.958	1.777
	1185.0	125.0	131.0	0.0158	11.768	9.9792	1.857	1.093	10.286	1.899	1.814	1.992
M2	∞	∞	∞	∞	∞	∞	1.930	1.210	9.870	1.981	2.112	1.838
	1185.0	125.0	131.0	∞	∞	∞	1.831	1.065	10.268	1.874	1.768	1.990
	1185.0	125.0	131.0	0.0158	11.768	9.9792	1.832	1.027	10.706	1.876	1.651	2.122

In Table 5, the first and fourth lines are the initial results that use infinite AVR and interstitial permeabilities. The osmolality, salt and urea concentrations ratios between bottom ($x = 1$) and top ($x = 0$) are given in the last six columns. It is evident that, for both M1 and M2, the urea concentration ratios increase if AVR permeabilities and interstitial permeability functions are included in the computational process.

If the standard deviations in the parameter values, given in Table 2, are used to put linear ramps with positive slopes on the urea permeabilities, then we get the results shown in Table 6. In this case, by comparing the first and fourth lines, and also, the fifth and eighth lines, we see that there is some improvement in the urea concentration ratios in CD.

Table 6. Osmolality and concentration ratios with linear ramps on permeabilities.

			DHL (Tube 1)			CD (Tube 3)		
	Δh_u^{AHL}	Δh_u^{DRV}	Osm.	Salt	Urea	Osm.	Salt	Urea
M1	0	0	1.853	1.197	9.087	1.909	2.139	1.657
	1.5×10^{-5}	0	1.860	1.201	9.126	1.916	2.146	1.664
	0	11.0×10^{-5}	1.913	1.211	9.648	1.970	2.161	1.762
	1.5×10^{-5}	11.0×10^{-5}	1.919	1.215	9.684	1.976	2.167	1.768
M2	0	0	1.726	1.033	9.368	1.775	1.824	1.722
	1.5×10^{-5}	0	1.731	1.035	9.401	1.780	1.829	1.727
	0	11.0×10^{-5}	1.738	1.034	9.496	1.788	1.826	1.745
	1.5×10^{-5}	11.0×10^{-5}	1.743	1.037	9.528	1.793	1.831	1.751

Finally, we varied the relative distances from those in Table 1 to those given in Table 7. The resulting concentration ratios are also given in Table 7. Comparing the last three entries of the fifth line in Table 6 with the corresponding entries of the third line in Table 7, we see that there is again some improvement in the concentration ratios for CD.

Table 7. Relative distances A_{pi} and the corresponding osm. and con. ratios from M2.

	DHL	AHL	CD	DVR	AVR1	AVR2	AVR3	Osm.	Salt	Urea
DHL (1)	–	85	85	1.5	1.0	2.5	2.0	1.748	1.021	9.764
AHL (2)	–	–	85	3.0	1.0	1.5	3.0			
CD (3)	–	–	–	4.0	2.0	1.0	4.0	1.800	1.820	1.778
DVR (5)	–	–	–	–	2.0	4.5	1.0			
AVR1 (4)	–	–	–	–	–	2.0	2.0			
AVR2 (6)	–	–	–	–	–	–	4.0			

5. CONCLUDING REMARKS

It was pointed out in the first section that M1 was obtained from M0, our previous seven tube model described in [14]. The rationale for the development of M0 was to show that, with only minor variations in the parameter values, vasa recta models lead to similar osmolality and concentration ratios as the central core models [11,12,15]. The parameters used for model M0 in [14] had lead to, respectively, 1.537, 5.937, and 0.617, as the osmolality, salt and urea concentration ratios for CD. For the new set of parameters presented in this paper, the corresponding values from M0 are 1.820, 2.082, and 1.533. Clearly, this is a significant improvement. The salt and urea concentrations at the bottom of CD are, respectively, 0.229 and 0.347 mmol/ml, which are well within the ranges of values given in [16]. Furthermore, it follows from the last three entries of the first line in Table 5, that M1 leads to further improvements in the concentration ratios.

In Table 5, comparing the first and second lines, and also the fourth and fifth lines, it is clear that incorporating the AVR permeabilities in both models, M1 and M2, CD urea concentration ratios increase and CD salt concentration ratios decrease. Furthermore, comparing the second and third lines, and also, the fifth and sixth lines, we see that the inclusion of interstitial permeability functions leads to additional improvements. These are very desirable results in terms of the renal concentrating mechanism since they are closer to the currently known experimental values than the results from previous models.

We have also shown in Table 6 that a linear ramp on permeabilities, using the standard deviations from Table 1, also leads to some improvements in the concentration ratios. Furthermore,

changing the distance functions between the tubes, from the values in Table 1 to Table 7, also leads to some improvements shown in the last three columns of Table 7.

Using permeabilities, reflection coefficients and boundary values that are within the ranges of experimentally known results, we have shown that our models give realistic concentration profiles and outputs.

REFERENCES

1. R.L. Jamison and W. Kriz, *Urinary Concentrating Mechanism: Structure and Function*, Oxford University Press, New York, (1982).
2. E. Koushanpour and W. Kriz, *Renal Physiology*, Second edition, Springer-Verlag, (1986).
3. W. Kriz, Structural orginization of the renal medullary counterflow system, *Fed. Proc.* **42** (8), 2379–2385, (1983).
4. W. Kriz and B. Kaisling, Structural organization of the kidney, In *The Kidney: Physiology and Pathophysiology*, (Edited by D.W. Seldin and G. Giebisch), 2nd edition, Raven Press, New York, (1992).
5. K.V. Lemley and W. Kriz, Cycles and separations: The histotopography of the urinary concentrating process, *Kidney Internat.* **31**, 538–548, (1987).
6. J.L. Stephenson, Models of the urinary concentrating mechanism, *Kidney Int.* **31**, 646–661, (1987).
7. J.L. Stephenson, Urinary concentration and dilution: models, In *Handbook of Physiology*, (Edited by E. Windhager), Chapter 30, pp. 1349–1408, Oxford University Press, New York, (1992).
8. H.E. Layton, Distribution of Henle's loops may enhance urine concentrating capability, *Biophys. J.* **49**, 1033–1040, (1986).
9. H.E. Layton and J.M. Davies, Distributed loops of henle in a central core model of the renal medulla: Where should the solute come out?, *Mathl. Comput. Modeling* **14**, 533–537, (1990).
10. P. Lory, A. Gilg and M. Horster, Renal countercurrent system: Role of collecting duct convergence and pelvic urea predicted from a mathematical model, *J. Math. Biology* **16**, 281–304, (1983).
11. J.L. Stephenson, J.F. Jen, H. Wang and R.P. Tewarson, Convective uphill transport of NaCl from ascending thin limb of the loop of Henle, *Amer. J. of Physiology* **268** (4), F680–F692, (1995).
12. J.L. Stephenson, H. Wang and R.P. Tewarson, Effect of vasa recta flow on concentrating ability of the renal inner medulla, *Amer. J. of Physiology* **268** (4), F698–F709, (1995).
13. R.P. Tewarson and I.H. Moon, Efficient computational algorithms for kidney modeling, In *Applied Sciences, especially Mechanics (Minisymposia), ZAAM* (Edited by E. Kreuzer and O. Mahrenholtz) (4), 51–54, (1996).
14. R.P. Tewarson and I.H. Moon, Renal concentrating mechanism: Central core and vasa recta models, *Appl. Math. Lett.* **10** (2), 39–44, (1997).
15. J.F. Jen, H. Wang, R.P. Tewarson and J.L. Stephenson, Comparison central core and radially separated models of the renal inner medulla, *Amer. J. of Physiology* **268** (4), F693–F697, (1995).
16. J. Lee, T. Morgan and P.G. Williams, Sodium and urea concentrations in renal papillary fluid of rats, with dehydration and vasopressin (pitressin) administration, *J. Physiol.* **215**, 41P–42P, (1971).
17. R.P. Tewarson, H. Wang, J.L. Stephenson and J.F. Jen., Efficient solution of differential equations for kidney concentrating mechanism analyses, *Appl. Math. Lett.* **4** (6), 69–72, (1991).
18. R.P. Tewarson, J.L. Stephenson and L.L. Juang, A note on solution of large sparse systems of nonlinear equations, *J. Math. Anal. and Appl.* **63**, 439–445, (1978).
19. K. Sun, I.H. Moon, R.P. Tewarson and J.L. Stephenson, Parallel algorithms for multi-nephron renal medullary models, *Computers Math. Applic.* **33** (6), 37–45, (1997).
20. M. Imai, Function of the thin ascending limb of Henle of rats and hamsters perfused in vitro, *Am. J. Physiol.* **232** (3), F201–F209, (1977).
21. M. Imai, J. Taniguchi and K. Yoshitomi, Transition of permeability properties along the limb of long-loop nephron, *Am. J. Physiol. (Renal Fluid Electrolyte Physiol.)* **254** (23), F323–F328, (1988).
22. T. Pallone, Effect of sodium cloride gradients on water flux in rat descending vasa recta, *J. Clin. Invest* **87**, 12–19, (1991).
23. T.L. Pallone, Transport of sodium chloride and water in rat ascending vasa recta, *Am. J. Physiol.* **261** (30), F519–F525, (1991).
24. T.L. Pallone, J. Work and R.L. Jamison, Resistance of descending vasa recta to the transport of water, *Am. J. Physiol.* **259** (28), F688–F697, (1990).
25. T.L. Pallone, J. Work, R.L. Myers and R.L. Jamison, Transport of sodium and urea in outer medullary descending vasa recta, *J. Clin. Invest.* **93**, 212–222, (1994).
26. J.M. Sands, H. Nonoguchi and M.A. Knepper, Vasopressin effects on urea and H_2O transport in inner medullary collecting duct subsegments, *Am. J. Physiol.* **253** (22), F823–F832, (1987).
27. J.M. Sands, H. Nonoguchi and M.A. Knepper, Hormone effects on NaCl6 permeability of rat inner medullary collecting duct, *Am. J. Physiol.* **255** (24), F421–F428, (1988).
28. R.P. Tewarson, W. Toro and M. Marcano, Preferential interaction and inverse problem algorithms in models of renal concentrating mechanism, *Appl. Math. Lett.* **11** (3), 51–59, (1998).

29. O. Kedem and A. Katchalsky, Permeability of composite membranes 3 series array of elements, *Trans. Faraday Soc.* **59**, 1941–1953, (1963).
30. E. Koushappour, R.R. Tarica and W.F. Stevens, Mathematical simulation of normal nephron function in rat and man, *J. Theor. Bio.* **31**, 177–214, (1971).